Taylor & Francis
Taylor & Francis Group

Check for updates

RESEARCH ARTICLE

Reckoning γ-Glutamyl-S-allylcysteine as a potential main protease (m^pro) inhibitor of novel SARS-CoV-2 virus identified using docking and molecular dynamics simulation

Arun Parashar[a], Arpit Shukla[b,c], Ankush Sharma[d], Tapan Behl[e], Dweipayan Goswami[f] and Vineet Mehta[e] (ID)

[a]Faculty of Pharmaceutical Sciences, Shoolini University of Biotechnology and Management Sciences, Solan, India; [b]Department of Biological Sciences, Institute of Advanced Research, Gandhinagar, India; [c]Department of Microbiology & Biotechnology, University School of Sciences, Gujarat University, Ahmedabad, India; [d]Department of Biotechnology, Yeshiva University, New York, NY, USA; [e]Department of Pharmacology, Chitkara University, Punjab, India; [f]Department of Pharmacology, Govt. College of Pharmacy, Rohru, India

ABSTRACT

Severe acute respiratory syndrome coronavirus-2 (SARS-CoV-2 or COVID-19), outbreak was first reported in December 2019 in the Wuhan, China. COVID-19 managed to spread worldwide and so far more than 9.1 million cases and more than 4.7 lakh death has been reported globally. Children, pregnant women, elderly population, immunocompromised patients, and patients with conditions like asthma, diabetes, etc. are highly vulnerable to COVID infection. Currently, there is no treatment available for COVID-19 infection. Traditional medicinal plants have provided bioactive molecules in the past that are efficiently used during conditions like cancer, malaria, microbial infections, immune-compromised states, etc. AYUSH India has recommended the use of *Curcuma longa, Allium sativum, Ocimum tenuiflorum,* and *Withania somnifera* for immune-boosting during SARS-CoV-2 infection. In the present study, we investigated the potential of 63-major bioactive molecules of these plants against SARS-CoV-2 main protease (M^pro) through docking studies and compared the results with known inhibitor 11a. Our results proposed cuscohygrine, γ-Glutamyl-S-allylcysteine, anahygrine, and S-allylcystein as the potent inhibitors against M^pro identified using molecular docking and molecular simulation dynamics. Interestingly, these molecules are from *A. sativum,* and *W. somnifera,* which are known for their antimicrobial and immunomodulatory potential. None of the proposed molecules have earlier been reported as antiviral molecules. Our results predict very strong potential of these four-molecules against SARS-CoV-2 M^pro, especially γ-glutamyl-S-allylcysteine, as all four form hydrogen bonding with Glu166 that is a crucial residue for the formation of the biologically active dimeric form of M^pro. Therefore, we strongly recommend further research on these biomolecules against SARS-CoV-2.

Introduction

Past two decades have witnessed the widespread health complications due to infections caused by Coronaviruses. These viruses are non-segmented positive sense RNA viruses belonging to the family of *Coronaviridae* and the subfamily of *Orthocoronaviridae* under superfamily of *Nidovirales* [1]. Initially, Coronaviruses were divided into the three groups (1, 2, and 3) based on their antigenic reactivity and variations in the genomic sequences. Recently, International Committee on Taxonomy of Viruses proposed new classification for the Coronaviruses in which they are divided into three genera, α-coronaviruses, β-coronaviruses and γ-coronaviruses, which corresponds to the group 1, 2 and 3 in the previous classification [2,3].

Coronaviruses are known to cause variety of infections in both, animals and humans, primarily targeting the respiratory system. In humans, coronaviruses are known to cause variety of minor infections such as common cold. HCoV-229E and HCoV-OC43 were the first two coronaviruses reported in humans [4], followed by HCoV-HKU1 and HCoV-NL63 [5]. All these four viruses rarely cause medical emergencies (unless associated with comorbid disease conditions) and are known to cause acute upper respiratory tract infections more frequently than lower respiratory tract infections [6,7]. Human coronaviruses (HCoV) are also capable of causing severe respiratory tract infection, of which zoonotic Severe Acute Respiratory Syndrome Coronavirus (SARS-CoV) and The Middle East Respiratory Syndrome Coronavirus (MERS-CoV) are best known [8]. SARS-CoV and MERS-CoV are known to cause serve health complications in the past one and a half decade and were designated as global epidemics due to heavy loss of life caused due to their infections globally [9,10]. These viruses may prove lethal in special category patients, particularly infants, elderly, pregnant females, immunocompromised patients, and patients having history of respiratory disease [5]. Currently, there is no specific treatment and drugs available for countering coronavirus infections and human immunity remains the primary defense against these viruses [11,12].

Recently, world witnessed yet again global pandemic due to the coronavirus which has still not reached its peak if seen in

---

terms of global mortality. Novel Human Coronavirus Disease (COVID-19) outbreak was first reported in the December 2019 in the Wuhan city of the Hubei province in the central China [13,14]. Since then COVID-19 has managed to spread worldwide across 213 countries and territories with more than 9.1 million cases and more than 4.7 lakh death globally (as on 23rd June 2020). These figures are continuously increasing and are expected to go much higher in coming days, especially in countries like the United States of America, Brazil, Russia, Spain, United Kingdom and India, which have witnessed community spread of COVID-19. Due to the lack of effective treatment so far, the World Health Organization (WHO) has been actively involved in the development of diagnostic tools and issuing guidelines for treatment procedures, patient care, prevention and monitoring, besides, promoting research for developing an effective drug/vaccine for the treatment of COVID-19 [15]. The virus, believed to be originated in bats, has now been known to primarily infect human respiratory system through human-to-human transmission *via* respiratory droplets and direct contact [6,14].

Since, there is no drug or vaccine available for the treatment of COVID-19, the concept of drug repurposing with oral Hydroxychloroquine has shown some positive effects in some reports. Moreover, the hunt for identifying novel targets to prevent replication of the SARS-CoV-2 is ongoing. This has led to the identification of several nonstructural SARS-CoV-2 proteins, which includes main protease (M[pro]), Nonstructural protein 10 (nsp10), nsp12, helicase (nsp13), N-terminal exoribonuclease and C-terminal guanine-N7 methyl transferase (nsp14), Uridylate-specific endoribonuclease (nsp15), 2′-O-methyltransferase (nsp16), and RNA-dependent RNA polymerase (RdRp). These SARS-CoV-2 proteins function to replicate and pack the viral genome [16,17]. Blocking the functioning of these proteins which adversely affect the replication and packing of the SARS-CoV-2 genome, and therefore, these proteins are now being considered as the key targets for drug development against SARS-CoV-2 [17].

Development of an effective treatment will require months, which will result in a lot more mortality globally and will have disastrous economic effect. Therefore, the search for the effective molecules for the management of COVID-19 should be directed toward traditional medicinal plants [18,19]. The Ministry of Ayurveda, Yoga & Naturopathy, Unani, Siddha and Homoeopathy (AYUSH), India has taken an initiative to promote the use of medicinal plants used in traditional Indian system of medicines for the management of infections for the management of COVID-19. These plants include *Curcuma longa* (Turmeric), *Allium sativum* (Garlic), *Ocimum tenuiflorum* (Tulsi), and *Withania somnifera* (Ashwagandha). All these traditional medicinal plants are known to have variety of medicinal values which includes antiviral, anti-inflammatory, and immune-boosting potential [20–23]. Currently, here is lack of effective curative and preventive therapeutic measures against COVID-19 crises and the immune system of the infected person is the most effective remedy to fight against this virus during non-sever early stage and severe later stage of the viral infection. It is now evident that during the early non-severe stage of COVID infection immune system prevent the spread of virus and during sever later stages, strong immunity is known to restrict the harmful effects of cytokine storm syndrome. All the traditional medicinal plants recommended by the AYUSH to be used during COVID pandemic are reported in Ayurveda as Rasayana or immunomodulatory [24]. Considering the potential of these plants to curb COVID infection based on the traditionally accumulated knowledge, AYUSH India issued an advisory to use these plants to control the health crisis arising due to COVID infection [25]. However, the experimental evidence for their effectiveness against the COVID-19 is not yet established.

In our present study we selected these plants as per the recommendations of AYUSH, raditional medicinal values of these plants and for their oral efficacy (suggesting their use orally can be intended). We further identified the bioactive molecules present in these plants and subjected them to molecular docking study to identify molecules with potential anti-coronavirus effect by investigating their interaction energy and type of interactions in concerned enzyme of SARS-CoV-2. For this study, we selected the M[pro] of SARS-CoV-2. The M[pro] of SARS-CoV-2 is crucial for the viral gene replication and gene expression *via* proteolytic processing of replicase polyproteins. Targeting M[pro] can result in the inhibition of viral replication and therefore is an attractive target for drug design against SARS-CoV-2 [26–29].

Material and methods

Datasets

The x-ray crystal structure of the M[pro] of SARS-CoV-2 was selected from the PDB database. We selected the crystal structure of M[pro] (PDB Id: 6M0K) [26] with resolution 1.50 Å. The standard inhibitor for this binding cleft is identified as the 11a ({N}-[(2∼{S})-3-(3-fluorophenyl)-1-oxidanylidene-1-[[(2∼{S})-1-oxidanylidene-3-[(3∼{S})-2-oxidanylidenepyrrolidin-3-yl]propan-2-yl]amino]propan-2-yl]-1∼{H}-indole-2-carboxamide). 11a has already been established as the inhibitor of M[pro] and this was used as a positive control in our study. M[pro] is a homo dimer of which only one chain is available in this crystal structure. Table S1 depicts the dataset of potential bioactive molecules of *Curcuma longa, Allium sativum, Ocimum tenuiflorum,* and *Withania somnifera,* which were used for molecular docking investigations.

Ligand-Preparation

The selected bioactive molecules were prepared using the protocol "prepare protein" of Accelrys Discovery studio package (BIOVIA, 2016). The 3-D conformers of these bioactive molecules were generated and saved as mol2 format for further analysis. DFT minimization protocols of Gaussian16 was used to optimize the ligand geometry [30,31]. The optimized molecules were then used for the docking analysis.

Molecular Docking

Molecular docking studies were performed using the SeeSAR version 9.2. Ligand binding site and the coordinates for the docking of the test compounds was kept same as for the positive control of the M[pro], 11a. The binding affinities of the selected bioactive molecule with the M[pro] of SARS-CoV-2 were calculated by the Hydrogen dehydration (HYDE) scoring function of the software [32,33]. The estimated binding affinity in SeeSAR ranges from mM < μM < nM < pM. In our study, the selection of the best scoring models was dependent on various parameters, such as Ligand Efficiency (LE), estimated binding affinity, and Torsion [34]. Moreover, the scoring function of HYDE depends on atom type-specific hydration and desolvation terms, which were conservatively aligned by Octanol to water partition coefficients (Kow) of small molecules. The water molecules which were residing inside the ligand were expelled out and water molecules which were

around the ligand were removed. This removed the chances of H-bond interactions between water molecules and protein or ligands, which may have resulted in a disfavored enthalpic contribution. Further, this formation of new H-bonds between the ligands and the target protein resulted in the compensation of the loos of energy as a result of water molecule removal. Unfavorable energy due to hydrophobic interactions between ligands and target protein prompt the breakage of H-bonds. Moreover, the energy of the ligand-protein complex was increased due to the removal of water molecules from the hydrophobic pockets of the complex and this phenomenon known as the hydrophobic impact [32,33]. An important drug-like parameter, the Lipophillic Ligand Efficiency (LLE), was calculated by merging the *in-vitro* binding strength of a ligand and lipophilicity [35]. The LE indicate the potency per atom and it is numerically calculated as the quotient of ΔG and the number of non-hydrogen atoms of the compound [36]. After completion of the molecular docking analysis, all the complexes were analyzed on basis of their binding affinity, LE, and Torsion values and the top most molecules were selected.

Molecular dynamics (MD) simulation

The best two ligands predicted from the docking study were used for the molecular dynamics simulation of M^pro in the presence of 11a using GROMACS 2019 software [37–39]. All the test docked complexes were compared with the 11a-M^pro docked complex (taken as control). SwissParam was used to generate the topology of the ligands. This provided us with the parameters and topology for test molecules compatible with CHARMM all atoms force field, for use with CHARMM and GROMACS [40]. The topology of the protein was created using GROMACS utilities using CHARMM27 all-atom force field (CHARM22 plus CMAP for proteins) with the water model set to TIP 3-point. The Ligand-protein complex were defined with unit cell box under periodic boundary conditions using 1.0 nm distance from the protein to the box faces with triclinic shape and was filled with water [41]. Further, Na^+ and Cl^- counter ion neutralization was performed along with the energy minimization to equilibrate the system under NVT (constant particle number, constant volume and constant temperature) for 25 ns at 300 K. After completion of the NVT run, the system was proceeded with NPT (constant particle number, constant volume and constant temperature) simulation and the molecular dynamics run was performed for 25 ns. LINCS or Linear Constraint Solver algorithm was used to constrain all the covalent bonds [42] and the PME or Particle Mesh Ewald method was used to treat the electrostatic interactions. The cutoff radii for the van der Waals and Coulomb interactions were set at 14.0 Å and 10.0 Å respectively. Trajectories were recorded after completion of NPT and NVT simulations and were analyzed for root-mean-square fluctuation (RMSF), root-mean-square deviation (RMSD), number of Hydrogen bonds formed between the ligand and M^pro protein, and radius of gyration (Rg) by using the 'gmx rmsf', 'gmx rms', 'gmx hbond' and gmx gyrate'of GROMACS utilities [37–39]. The stabilkity of the Ligand–protein complex was determined by the dynamics of ligand-protein hydrogen bonds with respect to time. Graphs were prepared using the XMgrace tool.

Binding free energy calculations MM/GBSA

The single trajectory approach was used for the binding free energy calculation using molecular mechanics generalized Born surface area (MM/GBSA) [43–46]. MM/GBSA in PRIME module of Maestro 11.4 was used to calculate the thermodynamic data of Coulomb energy (ΔGCoulomb), total free energy change (ΔGBind), Hydrogen-bonding correction (ΔGHbond), Pi-Pi packing correction (ΔGPacking), Lipophilic energy (ΔGLipo), and Van der Waals energy (ΔGvdW) for the trajectories obtained on performing MD simulations. MM/GBSA calculations were performed with the OPLS_2005 force field that use the VSGB 2.0 solvation model.

The free energy values were calculated using the following Equations (1) and (2):

$$\Delta G_{bind} = \Delta G_{complex(minimized)} - \left[\Delta G_{ligand(minimized)} + \Delta G_{receptor(minimized)} \right]$$ (1)

and

$$\Delta G_{bind} = \Delta G_{MM} + \Delta G_{GB} + \Delta G_{SA} - T\Delta S$$ (2)

where Δ_{TDS} is the conformation entropic contribution, and ΔG_{MM} is the molecular mechanics' interaction energy (electrostatic + van der Waals interaction) between protein and ligand. ΔG_{PB} and ΔG_{SA} depict the polar solvation energy and the nonpolar solvation energy, respectively.

In silico pharmacokinetic properties using ADMET analysis

In our study, we used the pkCSM - pharmacokinetics server [47] for predicting the absorption, distribution, metabolism, excretion, and toxicity (ADMET) properties of the top hits (Chloroquine, Cuscohygrine, γ-Glutamyl-S-allylcysteine, Anahygrine and S-allylcystein). This server predicted physiochemical as well as pharmacological properties. Simplified Molecule Input Line Entry Specification (SMILES) of the selected molecules were retrieved from PubChem, followed by uploading them to pkCSM - pharmacokinetics server. The server computed in-vivo absorption parameters like water solubility in the buffer system (SK atomic types, mg/L), Human intestinal absorption (HIA, %), in-vivo Caco2 cell permeability (Human colorectal carcinoma), in-vivo skin permeability (logKp, cm/hour), and in-vivo P-glycoprotein inhibition. We determined the metabolic parameters by using *in-vivo* Cytochrome P450 2C9 inhibition, in-vivo Cytochrome P450 2C19 inhibition, *in-vivo* Cytochrome P450 2D6 inhibition, in-vivo Cytochrome P450 3A4 inhibition, *in-vivo* Cytochrome P450 2D6 substrate, and in-vivo Cytochrome P450 3A4 substrate. For the distribution properties we included tests like, Blood-Brain Barrier (BBB) penetration, Central Nervous System (CNS) permeability and Lipinski's Rule (Rule of Five). To access the toxicity of compounds, a range of vital endpoints such as, ames test, acute algae toxicity, 2 years carcinogenicity bioassay in rat, 2 years carcinogenicity bioassay in mouse, *in-vivo* Ames test result in TA100 strain (Metabolic activation by rat liver homogenate) were computed. Moreover, many drugs are often withdrawn at clinical trial stages due to their poorer renal clearance, which makes excretion a very important parameter. Therefore, in this study we also included total renal clearance and renal OCT2 Substrate to identify the excretion efficacy of the molecules under study.

Results and discussion

Docking and interaction studies

The search for the bioactive molecules for the management of COVID-19 infection is ongoing throughout the world. The traditional drug screening process is highly time consuming with huge financial constraints, and has low degree of success rate. The availability and utilization of docking techniques has significantly reduced the screening time and have delivered good

results in recent past [48,49]. Bioactive molecules from various plants show extensive diversity in their chemical and structural properties, which opens up a vast area of research for exploration of their effects on the target sites of various proteins involved in several ailments, including COVID-19. For example, a recent study demonstrated that the bioactive molecules from the Tea plant, viz. Theasinensin-D, Oolonghomobisflavan-A, and Theaflavin-3-O-gallate, possess better binding affinity toward M^{pro} site of SARS-CoV-2, when compared to atazanavir, darunavir and lopinavir [48], making these molecules as point of interest for COVID research.

Molecular docking techniques are used to predict the binding sites on the target proteins (or receptors) and then explore the binding affinity of the ligand (drug under consideration) with the target protein [19,50]. Docking studies can simultaneously investigate thousands of molecules and rank them according to their binding affinities by taking into consideration multiple factors involved in ligand-drug interaction [49,51]. Further, high resolution crystallographic structure of RdRp-RNA complex has unlocked vast possibilities in the screening of antiviral drugs targeting a specific protein of SARS-CoV-2 [48,52]. The present study was aimed to explore the potential of bioactive molecules from the medicinal plants, which were recommended to be beneficial against COVID-19 by the AYUSH India, for their potential against SARS-CoV-2 M^{pro}. We identified the bioactive molecules (Table S1) of *C. longa, A. sativum, O. tenuiflorum,* and *W. somnifera* and screened for their potential against SARS-CoV-2 M^{pro}.

A total of 63 bioactive molecules along with Chloroquine were identified and compared with internal standard 11a for their binding affinities against the active site of SARS-CoV-2 M^{pro} protein (Table S2). Reports suggest that chloroquine is having beneficial effect during SARS-CoV-2 infection and is having a good potential to target SARS-CoV-2 M^{pro} protein [53–56]. The docking results of best four molecules, compared to Chloroquine, are depicted in Table 1 in terms of estimated affinity (Ki), ligand efficiency (LE), lipophilic ligand efficiency (LLE), and Torsion values. Cuscohygrine, γ-Glutamyl-S-allylcysteine, anahygrine, and S-allylcystein were selected on the basis of their estimated binding affinity against M^{pro} of SARS-CoV-2 (Table S2 and Table 1), and their chemical structures are depicted in Table 2.

SARS-CoV-2 M^{pro} is having a total of four binding sites, S1', S1, S2, and S4, and the 11a molecule is known to inhibit the activity of the SARS-CoV-2 M^{pro} by interacting at the S1' site of this protein [26]. Docking analysis for the test molecules was performed on the coordinates corresponding to S1' site of M^{pro}. We observed that 11a molecule is capable of interacting with the multiple amino acids at the S1' site of M^{pro}, which include hydrogen

bonding with Gly143, Cys145, and Glu166; Pi-Pi stacking with Leu141, Met165, and Pro168; Pi-sigma interaction with His41, and Met49; and Halogen interactions with Arg188, and Gln189. These results are depicted in the Figure 1. Interaction with the Cys145 is regarded as the crucial amino acid for inhibiting the activity of M^{pro}, as demonstrated in our results for the 11a-M^{pro} interaction [26]. It is worth mentioning that the 11a is a large molecule and was developed using computer aided drug design. It can inhibit the SARS-CoV-2 in *in-vitro* conditions, but may pose a threat to human life if administered. This is a major limitation of 11a which has led to divert the search for potential safer inhibitors toward the molecules of natural origin and/or molecules which are already being used clinically (drug repurposing). Chloroquine is one of the example of drug repurposing. It was used during SARS-CoV-2 infection and has shown some positive results to suppress the progression of viral infection. The docking pose of chloroquine within the active site of SARS-CoV-2 M^{pro} are depicted in Figure 2. Chloroquine binds to the active pocket of M^{pro} with an estimated affinity between 553.5 µM–54.9 mM. Both the LLE and LE parameters of molecular docking were very low for chloroquine in the binding site of M^{pro}. The binding was supported by favorable Torsion values. Moreover, Chloroquine formed a hydrogen bond with residues Asn142, His164 and Pi/Pi-alkyl interactions with residue His41 while formed Pi-Sulfur bond with Met165 of the M^{pro} of SARS-CoV-2.

Based on the estimated affinity of Chloroquine (553.5 µM − 54.9 mM), we selected four molecules, viz. cuscohygrine, γ-glutamyl-S-allylcysteine, anahygrine, S-allylcystein, based on their binding affinities as depicted in Table 2. The docking poses of these molecules within the active site of SARS-CoV-2 M^{pro} are depicted in Figure 2. Cuscohygrine, γ-glutamyl-S-allylcysteine, anahygrine, and S-allylcystein binds to the active pocket of M^{pro} with an estimated affinity between 1.20 µM − 120.1 µM, 18.7 µM − 1.86 mM, 14.3 µM- 1.42 mM, and 313.6 µM- 31.5 mM respectively. The LLE and LE parameters of molecular docking for all molecules were higher than chloroquine. LLE and LE parameters for γ-glutamyl-S-allylcysteine were observed to be higher than the rest of the molecules in the binding site of M^{pro}. The binding for all the natural molecules was also supported by favorable Torsion values. Amino acid interaction study of Anahygrine showed that it poorly interacts with the protein. It makes five bonds of which it forms only one H-bond. Cuscohygrine formed a hydrogen bond with residues Gly143 and Asn142, Pi Sulfur interaction Glu166. S-Allylcysteine and γ-glutamyl-S-allylcysteine showed the most promising results. S-Allylcysteine formed five H-bonds, namely with Asn142, Ser144, Gly143, Cys145 and His163; formed pi-alkyl interaction with Leu27. Here more importantly, this compound

Table 1. Interaction of the natural bioactive molecules with main protease (M^{pro}) of SARS-CoV-2.
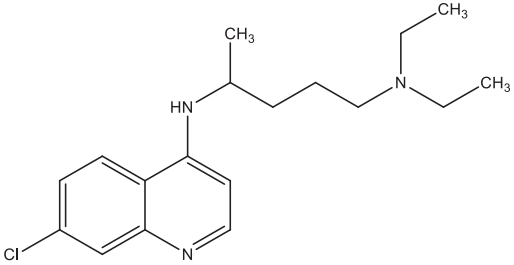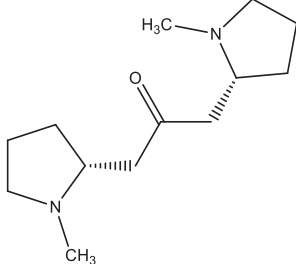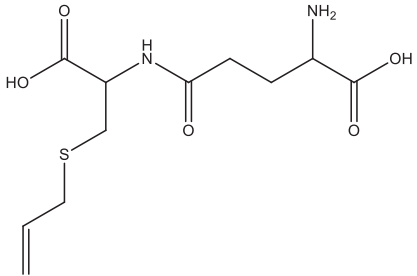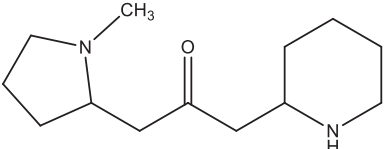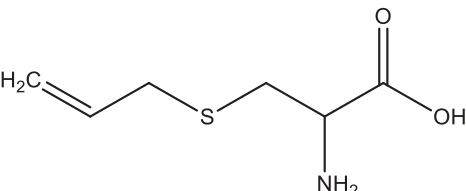
Ligand Name	LLE	LE	Range of Estimated Affinity (Ki)	Torsion
Chloroquine (standard drug)	👎	👎	553.5 µM − 54.9 mM	🟠
Cuscohygrine	👍	👍	1.20 µM − 120.1 µM	🟠
γ-Glutamyl-S-allylcysteine	👍	👍	18.7 µM − 1.86 mM	🟠
Anahygrine	👍	👍	14.3 µM − 1.42 mM	🟢
S-Allylcystein	👍	👍	313.6 µM − 31.5 mM	🟠

Table 2 The chemical structures and docking results of the top compounds.

S. No.	Name	Structure	Range of Estimated Affinity (Ki)
1.	Chloroquine		553.4 μM − 54.9 mM
2.	Cuscohygrine		1.20 μM − 120.1 μM
3.	γ-Glutamyl-S-allylcysteine		18.7 μM − 1.86 mM
4.	Anahygrine		14.3 μM − 1.42 mM
5.	S-allylcystein		313.6 μM − 31.5 mM

formed a hydrogen bond with Cys145, making this compound an impressive candidate as an inhibitor of M^{pro}. γ-glutamyl-S-allylcysteine showed the most optimum interaction with M^{pro} as it could make multiple interactions. It made in total six hydrogen bonds, involving five amino acids. These amino acids are His164, Glu166, Gln189, Arg188 and Thr190. Gln129 made unfavorable donor interaction, His163 formed Pi-alkyl interaction and Met165 formed carbon-hydrogen bond (Figure 3).

Molecular dynamics simulation

We conducted molecular dynamics simulations for different protein–ligand complexes, which includes positive control 11a-M^{pro}, S-Allylcysteine-M^{pro}, γ-glutamyl-S-allylcysteine-M^{pro} individually and their results were compared. S-Allylcysteine and γ-glutamyl-S-allylcysteine were selected for molecular dynamics simulation

based on the docking interaction observed with the M^{pro}. Our results demonstrated the good overall stability of the M^{pro} proteins in presence of the inhibitors being tested, S-Allylcysteine and γ-glutamyl-S-allylcysteine, in comparison 11a. The stability of the model system was checked using the RMSD, RMSF, hydrogen bonds formed, and by evaluating the total energy of the ligand-protein complex along the changes in pressure and temperature during the course of simulations.

RMSD is very crucial parameter to investigate the equilibrium of MD trajectories. RMSD of the protein backbone atoms is used to check the stability of ligand-protein complex during the simulations with respect to the time function. We calculated the RMSD values of the M^{pro} protein backbone against the simulation time scale (0–25) ns during its interaction with the internal ligand 11a, S-Allylcysteine and γ-glutamyl-S-allylcysteine (Figure 4).

The RMSD values of 11a-M^{pro} trajectories was least and could be sought to be the most stable interaction which ranged below
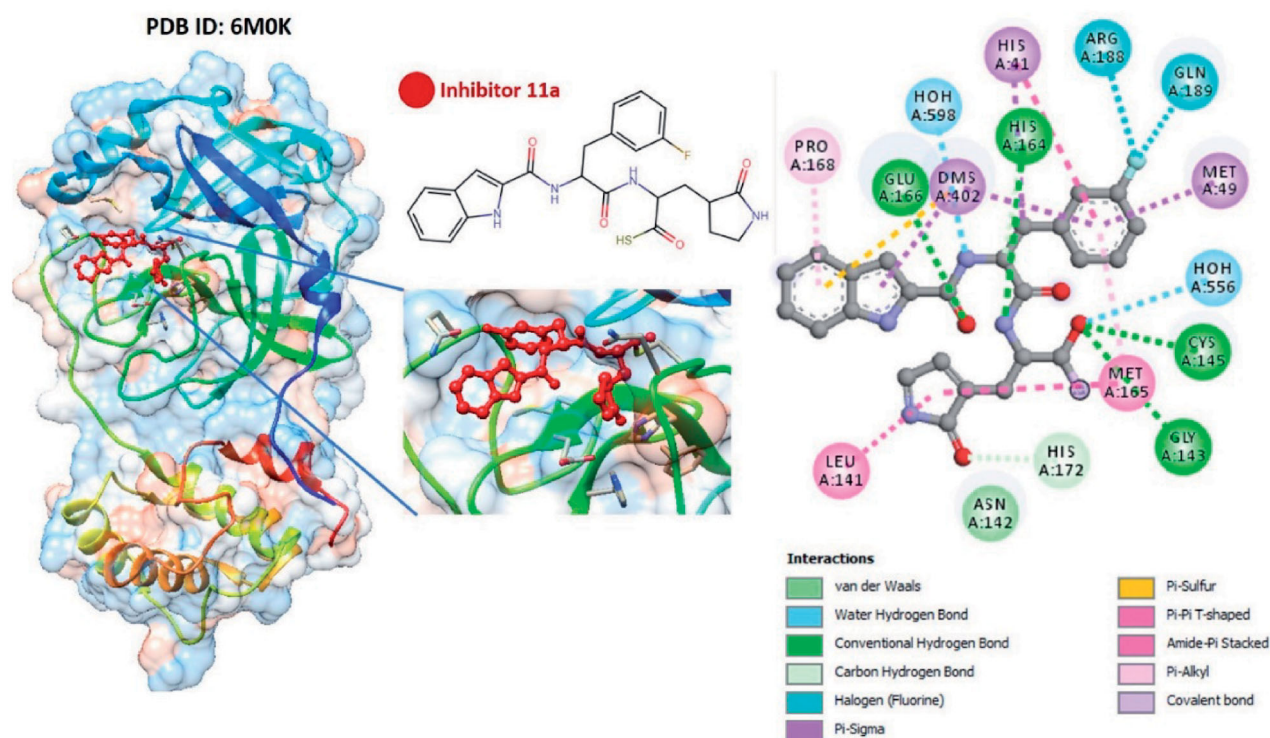
Figure 1. The interaction of 11a in the binding pocket of SARS-CoV-2 M^{pro} shown in two-dimensional, and in three-dimensional space.
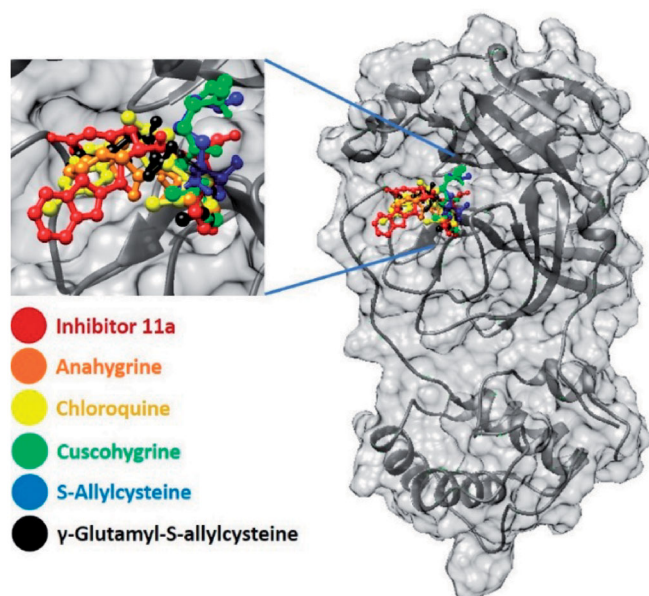

Figure 2. Superimposition of all the ligands at the S1' site of M^{pro}.

0.15 nm during simulation for the backbone of protein. While, S-Allylcysteine-M^{pro} interactions showed the RMSD to fluctuate for the first 5 ns of the simulation thereafter achieving stabilization and in this case the values never surpassed 0.6 nm. γ-glutamyl-S-allylcysteine-M^{pro} system showed much stabilized interactions as its RMSD values were much lower than that of S-Allylcysteine-M^{pro} complex and values under this case never surpassed 0.35 nm. However, despite there being differences in the ranges of RMSD fluctuations of all three systems, they all could be considered stable as none of the system showed RMSD values above 1 nm (Figure 4).

With respect to the average molecular dynamics simulation conformation, the RMSF reveals the means of portraying flexibility differences amongst various residues under investigation. The RMSF of the backbone atoms of each residue of (i) 11a-M^{pro} (as a positive control) and (ii) S-Allylcysteine-M^{pro} and (iii) γ-glutamyl-S-allylcysteine-M^{pro} individually was calculated to reveal the flexibility of the backbone structure in presence of both the ligands. This study indicates the behavior of protein in the presence of ligands under investigation. In this study, high RMSF value suggests greater flexibility and low RMSF value suggest the limited movements during simulation in relation to its average position. The RMSF of the residues are shown in Figure 5.

In the present study, we observed almost identical RMSF of the M^{pro} protein backbone in presence of all three molecules studied, suggesting the similar stability of protein. Moreover, RMSF values are higher when the binding is poor, which was definitely not the case in our studies (Figure 5). The inter-molecular hydrogen bonding between the ligand and protein is important for the stabilization on ligand-protein complex. The stability of the hydrogen bonds formed by all three molecules under investigation with M^{pro} was determined throughout the simulation at 300 K for the ligand system (Figure 6). The 11a-M^{pro} complex exhibited maximum of five H-bonds formation during the course of simulation. While for S-Allylcysteine-M^{pro}, there were consistently maximum of three hydrogen bonds being formed throughout the simulation study. But the results of docking were validated here in case of γ-glutamyl-S-allylcysteine, where this ligand could consistently make four to five H-bonds with M^{pro} throughout the course of simulation. Overall scenario suggests both natural ligands not only fits very well in to the binding cleft of 11a on S1' site of M^{pro}, but also make appropriate hydrogen bonds with the protein. Further, γ-glutamyl-S-allylcysteine is a much smaller molecule in comparison to 11a and is observed to make almost same number of H-bonds with the M^{pro} as made by 11a. Therefore the ratio of hydrogen bond to surface area is much greater for γ-glutamyl-S-allylcysteine compared to 11a, suggesting very strong interaction with M^{pro} in the S1' cleft. γ-glutamyl-S-allylcysteine, therefore, by
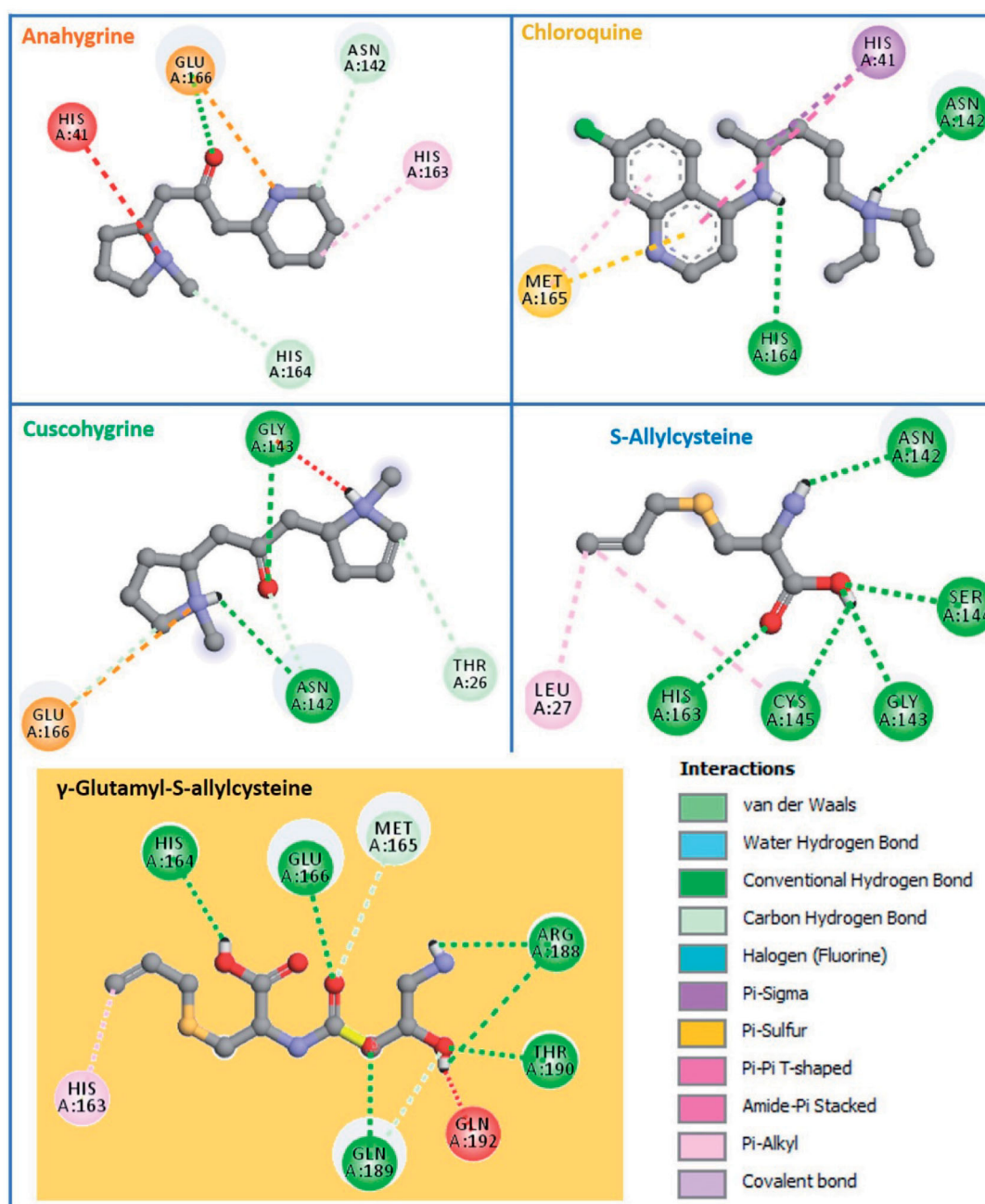
Figure 3. Interactions made by the Ligands under investigation with M^{pro}.

making enough hydrogen bonds to settle and block the space in the cleft might render the protein ineffective and this could be the key rationale behind its mode of action.

Molecular dynamics simulations performed at NVT reflects the stability of the ligand-protein complex in terms of the deviations from the pressure and temperature. In these studies, higher energy of the ligand-protein complex is undesirable and reflects the instability of the system.

From Figure 7(a) it is evident that all the three systems have almost identical total energy suggesting the similar stability of all the three systems i.e. 11a-M^{pro}, S-Allylcysteine-M^{pro}, and γ-glutamyl-S-allylcysteine-M^{pro}. Further, Figure 7(b) suggests the deviation in the temperature from the constant 300 K, where it is evident that the 11a-M^{pro} system has maximum deviation, this can be due to the large size of the ligand (11a) attached to the protein (M^{pro}). Since 11a is relatively larger in size and has more

possible interactions with M^{pro}, this could have resulted in the increased deviation in the overall temperature during simulations. Figure 7(c) suggests identical deviation in the pressure changes for all the three protein-ligand systems, suggesting their identical behavior in simulation. The results of the molecular dynamics simulations suggest that the protein behave in a similar way in presence of the all three ligand tested. Moreover, γ-glutamyl-S-allylcysteine can be considered as the best contender to serve as inhibitor of M^{pro} since this molecule showed maximum H-bond formation with M^{pro} along with stability corroborated by RMSD and RMSF values of a protein.

MM/Gbsa binding free energy calculations

MD trajectory analysis of both the trajectories with (i) M^{pro}-11a and (ii) M^{pro}- γ-Glutamyl-S-allylcysteine were performed to

understand the thermodynamic stability of the complexes which allows us to understand the spontaneity of the ligand receptor binding (Table 4). Binding free energy change calculation gives an estimate of that how strongly a ligand interact with the amino acids of the target protein. The energy released (ΔGbind) due to bond formation, or rath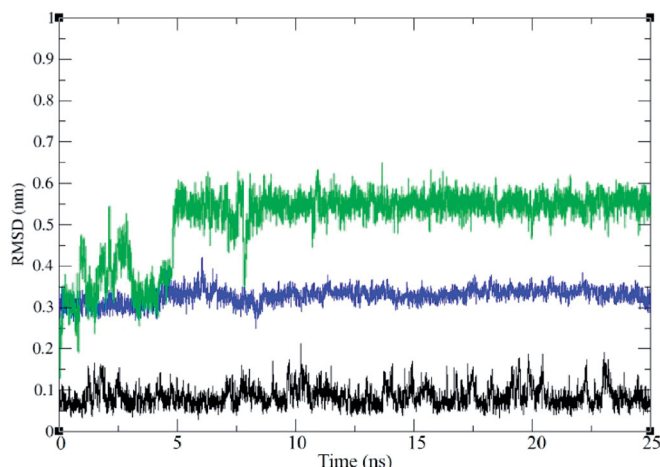er interaction of the ligand with protein is in the form of binding energy. This energy determines the stability of the protein–ligand complex under investigation. In our study, we observed that both ligands have ΔGBind in the negative range and shares the identical values. Moreover, both the compounds, tend to have similar energies corresponding to van der Waals interactions represented as ΔGvdW. These findings suggest that these compounds tends to stay in the vicinity of the interacting amino amides of M^{pro}. Further, both the compounds show negative values for Coulomb energy, suggests that these ligands while interacting with RBD has poor potential energy, suggesting better stability as the ligands do not have enough potential energy to get destabilized. In addition to the total energy, the contributions to the total energy from different components such as Lipophilic energy, Hydrogen-bonding correction, Pi-Pi packing correction and Van der Waals energy is depicted in Table 4. MM/GBSA analysis suggests that spontaneity of interaction forming capabilities of γ-Glutamyl-S-allylcysteine is at par with native ligand, 11a (well-established inhibitor).

Figure 4. Representation of ligand RMSD of M^{pro} backbone during interaction with internal standard 11a, S-Allylcysteine, and γ-glutamyl-S-allylcysteine during their interaction with M^{pro} of COVID-19 derived from NVT Simulation at 300 K.

ADMET analysis

All the ADMET properties of the top screened compounds along with GRL0617 is depicted in Table 3. For a compound to be classified as an oral drug, it is important to predict its mobility through the intestinal epithelial layers of cells that predicts the bioavailability. The theoretical model makes the use of Caco-2 permeability and its value higher than 0.90 means the compound has high
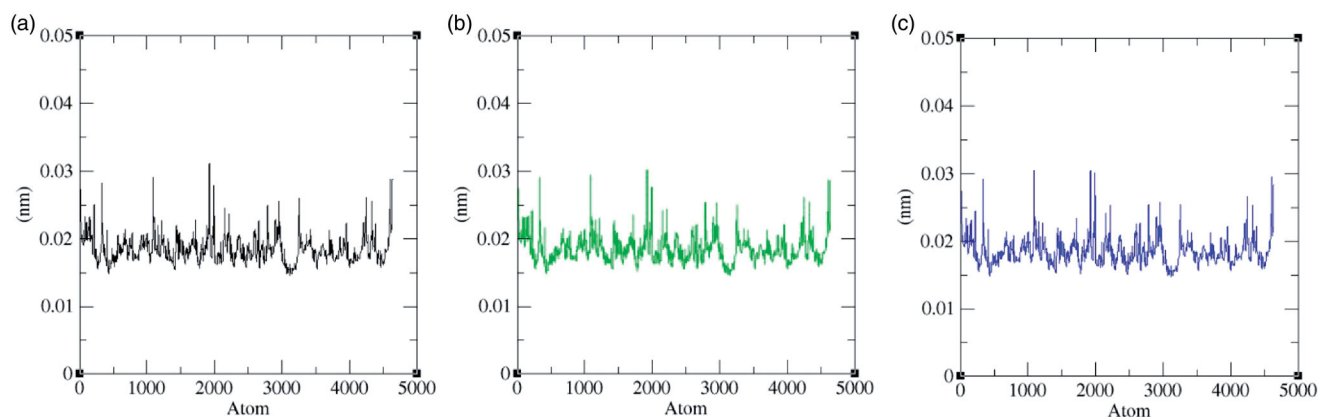

Figure 5. Representation of Molecular Dynamics (a) RMSF values of M^{pro} backbone during its interaction with 11a, (b) S-Allylcysteine (c) γ-glutamyl-S-allylcysteine during simulation.
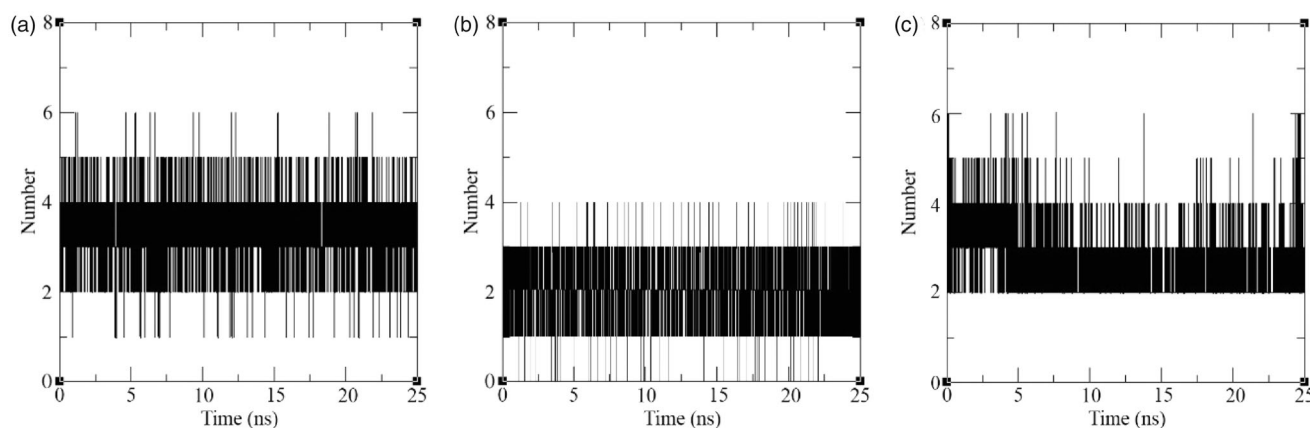

Figure 6. Representation of hydrogen bond formation of (a) 11a, (b) S-Allylcysteine (c) γ-glutamyl-S-allylcysteine, with M^{pro} during simulation.
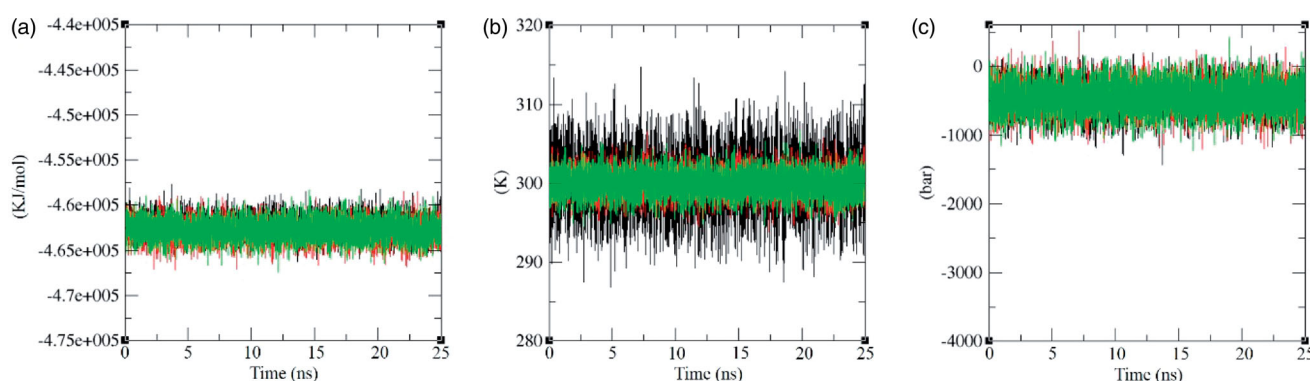
Figure 7. Representation of (a) total energy changes (b) Changes in the temperature of the system (c) changes in the pressure for the systems 11a-M^{pro}, S-Allylcysteine-M^{pro} (c) γ-glutamyl-S-allylcysteine-M^{pro} .

Table 3. ADMET Analysis of the Top Hits.

		Predicted Value					
Property	Model Name	Chloroquine	Cuscohygrine	γ-Glutamyl-S-allylcysteine	Anahygrine	S-allylcystein	Unit
Absorption	Water solubility		−1.108	−2.891	−1.121	−2.888	Numeric (log mol/L)
Absorption	Caco2 permeability	1.624	1.364	−0.517	1.349	0.704	Numeric (log Papp in 10^{-6} cm/s)
Absorption	Intestinal absorption (human)	89.95	94.096	8.312	93.917	79.971	Numeric (% Absorbed)
Absorption	Skin Permeability	−2.679	−2.984	−2.735	−3.054	−2.736	Numeric (log Kp)
Absorption	P-glycoprotein substrate	Yes	No	Yes	No	No	Categorical (Yes/No)
Absorption	P-glycoprotein I inhibitor	No	No	No	No	No	Categorical (Yes/No)
Absorption	P-glycoprotein II inhibitor	No	No	No	No	No	Categorical (Yes/No)
Distribution	VDss (human)	1.332	0.979	−0.48	0.957	−0.561	Numeric (log L/kg)
Distribution	Fraction unbound (human)	0.191	0.757	0.452	0.755	0.444	Numeric (Fu)
Distribution	BBB permeability	0.349	0.236	−1.124	0.225	−0.277	Numeric (log BB)
Distribution	CNS permeability	−2.191	−3.226	−4.02	−3.237	−3.417	Numeric (log PS)
Metabolism	CYP2D6 substrate	Yes	No	No	No	No	Categorical (Yes/No)
Metabolism	CYP3A4 substrate	Yes	No	No	No	No	Categorical (Yes/No)
Metabolism	CYP1A2 inhibitor	No	No	No	No	No	Categorical (Yes/No)
Metabolism	CYP2C19 inhibitor	No	No	No	No	No	Categorical (Yes/No)
Metabolism	CYP2C9 inhibitor	No	No	No	No	No	Categorical (Yes/No)
Metabolism	CYP2D6 inhibitor	Yes	No	No	No	No	Categorical (Yes/No)
Metabolism	CYP3A4 inhibitor	No	No	No	No	No	Categorical (Yes/No)
Excretion	Total Clearance	1.092	1.159	0.3	1.218	0.591	Numeric (log ml/min/kg)
Excretion	Renal OCT2 substrate	Yes	No	No	No	No	Categorical (Yes/No)
Toxicity	AMES toxicity	Yes	No	No	No	No	Categorical (Yes/No)
Toxicity	Max. tolerated dose (human)	−0.167	0.093	1.119	0.115	1.126	Numeric (log mg/kg/day)
Toxicity	hERG I inhibitor	No	No	No	No	No	Categorical (Yes/No)
Toxicity	hERG II inhibitor	Yes	No	No	No	No	Categorical (Yes/No)
Toxicity	Oral Rat Acute Toxicity (LD50)	2.85	2.385	2.438	2.407	2.02	Numeric (mol/kg)
Toxicity	Oral Rat Chronic Toxicity (LOAEL)	1.026	0.799	2.29	0.808	2.635	Numeric (log mg/kg_bw/day)
Toxicity	Hepatotoxicity	Yes	No	No	No	No	Categorical (Yes/No)
Toxicity	Skin Sensitization	No	Yes	No	Yes	No	Categorical (Yes/No)
Toxicity	*T. pyriformis* toxicity	1.558	0.291	0.285	0.227	0.166	Numeric (log ug/L)
Toxicity	Minnow toxicity	0.747	2.072	2.928	2.067	2.088	Numeric (log mM)

Table 4. MM/GBSA profiles of 11a, and γ-Glutamyl-S-allylcysteine, while interacting with M^{pro}.

Ligand	ΔGBind (Kcal/mol)	ΔGCoulomb (Kcal/mol)	ΔGHbond (Kcal/mol)	ΔGLipo (Kcal/mol)	ΔGPacking (Kcal/mol)	ΔGvdW (Kcal/mol)
11a	−61.834	−29.63	−2.59	−15.44	−2.25	−34.22
γ-Glutamyl-S-allylcysteine	−72.45	−28.71	−3.32	−20.53	−3.29	−37.67

permeability. Under present study all the compounds shows the Caco-2 permeability values in positive integer suggesting them to be absorbing through intestinal epithelial layers. The only exception is γ-Glutamyl-S-allylcysteine where the value is −0.517. Intestinal absorption (human) value is another parameter that calculates the absorption of the drug from human gut when administered orally. All the phytochemicals showed efficient intestinal absorption except γ-Glutamyl-S-allylcysteine. The next important parameter is skin permeability, where it was observed that all the compounds under study have values smaller than −2.5 log Kp,

which means these compounds have poor permeability. All the compounds under study showed identical skin permeability. The ATP-binding cassette (ABC) transporter is important for transport of molecules through cell membrane and P-glycoprotein is its component needed for efficient transport, and its value 'yes' predicts the compound to pass cell membrane through ABC transporter. Here, γ-Glutamyl-S-allylcysteine and Chloroquineare predicted to pass through the cell membrane *via* ABC transporters. Total diffusion of drug in total blood volume is determined by "volume of Distribution (VDss)" and its value below −0.15 logVDss

suggest poor diffusion while values higher than 0.45 LogVDss suggests faster and higher equal distribution of drug in the total blood volume. The ability of compound to travel to the brain is given by the values of Blood-Brain barrier (BBB) permeability. When the logBB values are greater than 0.3, they can pass BBB. Values of compounds under study predicted that all the compounds may not be able to cross BBB and this attribute was only found to be present by Chloroquine. Further, where none of the compounds except Chloroquine is predicted to show CYP1A2, CYP2C19, CYP2C9, CYP2D6 and CYP3A4 inhibition as analysis obtained from metabolism prediction, while Chloroquine is predicted to inhibit only CYP2D6. Renal excretion rate of all the compounds under study were different and no compound except Chloroquine predicted to show AMES toxicity which important to predict as this test suggest drug's property of mutagenicity. Potassium flux in heart is controlled by hERG I and II, improper flux of potassium by these transporters can cause QT syndrome where the Q and T peaks of heart electrocardiogram gets altered. The impact of screened compounds under present study on hERG I and II transporters are shown in Table 3 along with other essential ADMET properties.

Overall discussion of the docking and molecular dynamics results

The recent outbreak of the COVID-19 or the SARS-CoV-2 has initiated a worldwide hunt for the therapeutic molecule effective against the viral infection [14,16,17]. One of the most effective strategy for therapeutics of SARS-CoV-2 is to target viral transcription and replication. A biomolecule which is capable of inhibiting the viral replication and transcription would be the ideal molecule to control spread of COVID-19. M^{pro} has been identified as the play vital role in the viral transcription and replication, and therefore, ant biomolecule capable of this protein could possibly prevent the viral transcription and replication [26].

Cuscohygrine and anahygrine are the two major biomolecules present in the *W. somnifera*. Cuscohygrine is primarily used as a biomarker to distinguish a practice of cocaine abuse from coca chewing [57] and has never been identified or recognized for its antiviral potential. Likewise, anahygrine is also not known for any major health benefits or for antiviral potential. *W. somnifera* is known for variety of health benefits on variety of ailments, one of which being a potent immune booster and immune stimulator [58–60]. Further, a traditional Indian formulation (Amukkara Choornam) based on *W. somnifera* has been reported to show beneficial effects against Chikungunya Virus [61], suggesting the antiviral potential of this plant. The broad health benefits of this plant are due to the presence of diverse chemical constituents such as cuscohygrine and anahygrine. Investigating the efficacy of cuscohygrine and anahygrine against the SARS-CoV-2 might yield beneficial effects *via* its action on SARS-CoV-2 M^{pro}, as indicated by the findings of our docking studies.

γ-glutamyl-S-allylcysteine, and S-allylcystein are the major bioactive molecules of *A. sativum* (garlic). Although γ-glutamyl-S-allylcysteine is not explored much for its pharmacological actions, S-allylcystein is known to possess anticancer, antidiabetic, nephroprotective, and neuroprotective potential [62–64]. Our findings suggest that both molecules are having good activity against SARS-CoV-2 M^{pro} and need further investigation. Moreover, *A. sativum* is also recognized for its variety of health benefits, which includes anti-microbial effects and immune booster potential [63,65].

In this study we demonstrated that cuscohygrine, γ-glutamyl-S-allylcysteine, anahygrine, and S-allylcystein derived from Ashwagandha and Garlic binds to the active pocket of the M^{pro} of SARS-CoV-2. The binding was stabilized by hydrogen bonds, Pi/Pi-alkyl interactions, and favorable LE, LLE and Torsion values. Moreover, all four molecules formed a hydrogen bond with residue Glu166, a crucial residue for the formation of biologically active dimeric form of M^{pro}. Further, Pi/Pi-alkyl interactions with Cys145 also appears to be important for the interaction with M^{pro} of SARS-CoV-2 as this interaction was depicted by all molecules except cuscohygrine. Moreover, these results were confirmed through molecular dynamics simulations, where γ-glutamyl-S-allylcysteine demonstrated best results. Our findings suggest that in addition to the immunoboosting potential, these bioactive molecules could actively participate in combating the notorious coronavirus within the host body.

Conclusion

The present study was aimed at identifying the bioactive molecules for their potential against M^{pro} main protease of SARS-CoV-2 through molecular docking and molecular dynamics studies. In this study, we looked into the major bioactive molecules present in four medicinally important plants of India, viz. *C. longa, A. sativum, O. tenuiflorum,* and *W. somnifera*, which are recommended by the AYUSH, India for their beneficial effects against SARS-CoV-2 infection. Out of the 63 bioactive molecules, cuscohygrine, γ-glutamyl-S-allylcysteine, anahygrine, and S-allylcystein demonstrated potential against M^{pro} main protease and their activity was observed to be better than the chloroquine. All these molecules demonstrated hydrogen bonding with the Glu166 residue, which is a crucial residue for the formation of biologically active dimeric form of M^{pro}, suggesting that these molecules can target M^{pro} very efficiently. Further, molecular dynamics simulation studies confirmed our results and predicted γ-glutamyl-S-allylcysteine as the best molecule which could act on the M^{pro} of SARS-CoV-2. Interestingly, all these molecules are not known for their potential against viral infections. Moreover, these molecules are present in good quantity in *A. sativum* and *W. somnifera* and both these plants are known to possess immunomodulatory, immune-booster and immune-stimulatory potential, which could be because of these molecules. Our results also validate the recommendations of AYUSH India for the use of *A. sativum* and *W. somnifera* for SARS-CoV-2 and suggest the presence of cuscohygrine, γ-glutamyl-S-allylcysteine, anahygrine, and S-allylcystein in these plants may provide protection against SARS-CoV-2 infection by targeting M^{pro}. The proposed molecules, especially γ-glutamyl-S-allylcysteine, need to be investigated further for their potency against SARS-CoV-2. These molecules may find a clinical application, however, an intensive and rapid research is required.

ORCID

Vineet Mehta 🆔 http://orcid.org/0000-0003-0485-5076

References

[1] Richman D, Whitley R, Hayden F. Clinical virology. 2016. https://books.google.com/books?hl=en&lr=&id=G9zIDwAAQBAJ&oi=fnd&pg=PT8&dq=26.%09Richman,+D.+D.,+Whitley,+R.+J.,+%26+Hayden,+F.+G.+(2016).+Clinical+Virology.+John+Wiley+%26+Sons.&ots=FcgFv6n-FO&sig=EbNz-R7HQoV-m6GkdlQQxIQNpDQ.

[2] Pyrc K, Dijkman R, Deng L, et al. Mosaic structure of human coronavirus NL63, one thousand years of evolution. Elsevier. 2006. Retrieved July 9, 2020, from https://www.sciencedirect.com/science/article/pii/S0022283606012988.

[3] Schwartz DA, Graham AL. Potential maternal and infant outcomes from coronavirus 2019-NCOV (SARS-CoV-2) infecting pregnant women: Lessons from SARS, MERS, and other human coronavirus infections. Viruses. 2020;12(2):194.

[4] Van Der Hoek L, Pyrc K, Jebbink MF, et al. Identification of a new human coronavirus. Nat Med. 2004;10(4):368–373.

[5] Woo PCY, Lau SKP, Chu C-M, et al. Characterization and complete genome sequence of a novel coronavirus, coronavirus HKU1, from Patients with Pneumonia. JVI. 2005;79(2):884–895.

[6] Lau SKP, Patrick CYW, Yip CCY, et al. Coronavirus HKU1 and other coronavirus infections in Hong Kong. J Clin Microbiol. 2006;44(6):2063–2071.

[7] Reina J, López-Causapé C, Rojo-Molinero E, et al. Clinico-epidemiological characteristics of acute respiratory infections by coronavirus OC43, NL63 and 229E. Revista Clínica Española (English Edition). 2014;214(9):499–504.

[8] Drosten C, Günther S, Preiser W, et al. Identification of a novel coronavirus in patients with severe acute respiratory syndrome. N Engl J Med. 2003;348(20):1967–1976.

[9] Hui DS. Epidemic and emerging coronaviruses (severe acute respiratory syndrome and middle east respiratory syndrome). Clin Chest Med. 2017;38(1):71–86.

[10] Perlman S. Another decade, another coronavirus. N Engl J Med. 2020;382(8):760–762. Issue Massachussetts Medical Society.

[11] Song Z, Xu Y, Bao L, et al. From SARS to MERS, thrusting coronaviruses into the spotlight. Viruses. 2019;11(1):59.

[12] Wu F, Zhao S, Yu B, et al. A new coronavirus associated with human respiratory disease in China. Nature. 2020;579(7798):265–269.

[13] Zhou P, Yang XL, Wang XG, et al. A pneumonia outbreak associated with a new coronavirus of probable bat origin. Nature. 2020;579(7798):270–273.

[14] Zhu N, Zhang D, Wang W, et al.; China novel coronavirus investigating and research team. A novel coronavirus from patients with pneumonia in China, 2019. N Engl J Med. 2020;382(8):727–733.

[15] Munster VJ, Koopmans M, van Doremalen N, et al. A novel coronavirus emerging in China – Key questions for impact assessment. N Engl J Med. 2020;382(8):692–694.

[16] Jin Z, Du X, Xu Y, et al. Structure of M pro from SARS-CoV-2 and discovery of its inhibitors. Nature. 2020;582(7811):289–293.

[17] Kong R, Yang G, Xue R, et al. COVID-19 Docking Server: An interactive server for docking small molecules, peptides and antibodies against potential targets of COVID-19. J ArXiv Preprint. 2020. https://arxiv.org/abs/2003.00163

[18] Chen Z, Nakamura T. Statistical evidence for the usefulness of Chinese medicine in the treatment of SARS. Phytother Res. 2004;18(7):592–594.

[19] Rao P, Shukla A, Parmar P, et al. Reckoning a fungal metabolite, Pyranonigrin A as a potential Main protease (Mpro) inhibitor of novel SARS-CoV-2 virus identified using docking and molecular dynamics simulation. Biophys Chem. 2020;264:106425.

[20] Ali I, Alharbi OM. COVID-19: disease, management, treatment, and social impact. Sci Total Environ. 2020;728:138861–138866.

[21] AYUSH. Ayurveda's immunity boosting measures for self care during COVID 19 crisis. The Ministry of Ayurvedic, Yoga and Naturopathy, Unani, Siddha and Homeopathy 2020. http://ayush.gov.in/event/ayurveda-immunity-boosting-measures-self-care-during-covid-19-crisis.

[22] Kumar V, Dhanjal JK, Kaul SC, et al. Withanone and caffeic acid phenethyl ester are predicted to interact with main protease (Mpro) of SARS-CoV-2 and inhibit its activity. J Biomol Struct Dyn. 2020:1–13.

[23] Xu Y, Su D, Zhu L, et al. S-allylcysteine suppresses ovarian cancer cell proliferation by DNA methylation through DNMT1. J Ovarian Res. 2018;11(1):39.

[24] Kumar D, Arya V, Kaur R, et al. A review of immunomodulators in the Indian traditional health care system. J Microbiol Immunol Infect. 2012;45(3):165–184.

[25] Gautam S, Gautam A, Chhetri S, et al. Immunity against covid-19: potential role of Ayush Kwath. J Ayur Integr Med. 2020. DOI:10.1016/j.jaim.2020.08.003

[26] Dai W, Zhang B, Jiang XM, et al. Structure-based design of antiviral drug candidates targeting the SARS-CoV-2 main protease. Science. 2020;368(6497):1331–1335.

[27] Jin Z, Du X, Xu Y, et al. Structure of M pro from COVID-19 virus and discovery of its inhibitors. Nature. 2020;582(7811):289–293.

[28] Joshi RS, Jagdale SS, Bansode SB, et al. Discovery of potential multi-target-directed ligands by targeting host-specific SARS-CoV-2 structurally conserved main protease. J Biomol Struc Dyn. 2020;39(9):3099–3114.

[29] Kumar Y, Singh H, Patel CN. In silico prediction of potential inhibitors for the main protease of SARS-CoV-2 using molecular docking and dynamics simulation based drug-repurposing. J Infect Public Health. 2020;13(9):1210–1223.

[30] Parmar P, Shukla A, Rao P, et al. The rise of gingerol as anti-QS molecule: darkest episode in the LuxR-mediated bioluminescence saga. Bioorg Chem. 2020;99:103823.

[31] Zheng J, Frisch MJ. Efficient geometry minimization and transition structure optimization using interpolated potential energy surfaces and iteratively updated hessians. J Chem Theory Comput. 2017;13(12):6424–6432.

[32] Reulecke I, Lange G, Albrecht J, et al. Towards an integrated description of hydrogen bonding and dehydration: Decreasing false positives in virtual screening with the HYDE scoring function. ChemMedChem. 2008;3(6):885–897.

[33] Schneider N, Lange G, Hindle S, et al. A consistent description of HYdrogen bond and DEhydration energies in protein-ligand complexes: Methods behind the HYDE scoring function. J Comput Aided Mol Des. 2013;27(1):15–29.

[34] Wang W, Donini O, Reyes CM, et al. Biomolecular simulations: recent developments in force fields, simulations of enzyme catalysis, protein-ligand, protein-protein, and

protein-nucleic acid noncovalent interactions. Annu Rev Biophys Biomol Struct. 2001;30(1):211–243.

[35] Abad-Zapatero C. Ligand efficiency indices as guideposts for drug discovery. 2005. Retrieved July 9, 2020, from www.drugdiscoverytoday.com.

[36] Hopkins AL, Groom CR, Alex A. Ligand efficiency: a useful metric for lead selection. Drug Discov Today. 2004;9(10): 430–431.

[37] Bekker H, Berendsen HJC, Dijkstra EW, et al. Gromacs: a parallel computer for molecular dynamics simulations. Singapore: World Scientific Publishing; 1993.

[38] Pronk S, Páll S, Schulz R, et al. GROMACS 4.5: A high-throughput and highly parallel open source molecular simulation toolkit. Bioinformatics. 2013;29(7):845–854.

[39] Van Der Spoel D, Lindahl E, Hess B, et al. %J J. of computational chemistry. GROMACS. 2005;26(16):1701–1718.

[40] Zoete V, Cuendet MA, Grosdidier A, et al. SwissParam: a fast force field generation tool for small organic molecules. J Comput Chem. 2011;32(11):2359–2368.

[41] Berendsen HJC, Postma JPM, van Gunsteren WF, et al. Interaction models for water in relation to protein hydration. In: Intermolecular forces. Dordrecht, Netherlands: Springer; 1981. p. 331–342

[42] Hess B, Bekker H, Berendsen HJC, et al. LINCS: a linear constraint solver for molecular simulations. J Comput Chem. 1997;18(12):1463–1472.

[43] Kollman PA, Massova I, Reyes C, et al. Calculating structures and free energies of complex molecules: combining molecular mechanics and continuum models. Acc Chem Res. 2000;33(12):889–897.

[44] Massova I, Kollman PA. Combined molecular mechanical and continuum solvent approach (MM-PBSA/GBSA) to predict ligand binding. Perspect Drug Disc Design. 2000;18(1): 113–135.

[45] Wang J, Hou T, Xu X. Recent advances in free energy calculations with a combination of molecular mechanics and continuum models. CAD. 2006;2(3):287–306.

[46] Wang J, Wang W, Kollman PA, et al. Antechamber: an accessory software package for molecular mechanical calculations. J J. Am. Chem. Soc. 2001;222:U403.

[47] Pires DEV, Blundell TL, Ascher DB. PkCSM: predicting small-molecule pharmacokinetic and toxicity properties using graph-based signatures. J Med Chem. 2015;58(9): 4066–4072.

[48] Bhardwaj VK, Purohit R. Targeting the protein-protein interface pocket of Aurora-A-TPX2 complex: rational drug design and validation. J Biomol Struct Dyn. 2020:1–10.

[49] Lionta E, Spyrou G, Vassilatis DK, et al. Structure-based virtual screening for drug discovery: principles, applications and recent advances. Curr Topics Med Chem 2014;14. https://www.ingentaconnect.com/content/ben/ctmc/2014/00000014/00000016/art00008.

[50] Shukla A, Parmar P, Rao P, et al. Twin peaks: presenting the antagonistic molecular interplay of curcumin with LasR and LuxR quorum sensing pathways. Curr Microbiol. 2020;77(8): 1800–1810.

[51] Kumar V, Dhanjal J, Kaul S. Withanone and Caffeic Acid Phenethyl Ester are Predicted to Interact with Main Protease (Mpro) of SARS-CoV-2 and Inhibit its Activity. Taylor & Francis. 2020. Retrieved July 9, 2020, from https://www.tandfonline.com/doi/abs/10.1080/07391102.2020.1772108.

[52] Yang H, Bartlam M, Rao Z. Drug design targeting the main protease, the achilles' heel of coronaviruses. Curr Pharm Des. 2006;12(35):4573–4590.

[53] Braz HLB, de Moraes Silveira JA, Marinho AD, et al. In silico study of azithromycin, chloroquine and hydroxychloroquine and their potential mechanisms of action against SARS-CoV-2 infection. Int J Antimicrob Agents. 2020;56(3):106119.

[54] Li Z, Li X, Huang YY, et al. Identify potent SARS-CoV-2 main protease inhibitors via accelerated free energy perturbation-based virtual screening of existing drugs. Proc Natl Acad Sci USA. 2020;117(44):27381–27387.

[55] Rebeaud ME, Zores F. SARS-CoV-2 and the use of chloroquine as an antiviral treatment. Front Med. 2020;7:184.

[56] Singh AK, Singh A, Shaikh A, et al. Chloroquine and hydroxychloroquine in the treatment of COVID-19 with or without diabetes: A systematic search and a narrative review with a special reference to India and other developing countries. Diab Metab Syndr. 2020;14(3):241–246.

[57] Rubio NC, Thurmann D, Krumbiegel F, et al. Behaviour of hygrine and cuscohygrine in illicit cocaine production establishes their use as markers for chewing coca leaves in contrast with cocaine abuse. Drug Test Anal. 2017;9(2): 323–326.

[58] Vetvicka V, Vetvickova J. Immune enhancing effects of WB365, a novel combination of Ashwagandha (Withania somnifera) and Maitake (Grifola frondosa) extracts. N Am J Med Sci. 2011;3(7):320–324.

[59] Yamada K, Hung P, Park TK, et al. A comparison of the immunostimulatory effects of the medicinal herbs Echinacea, Ashwagandha and Brahmi. J Ethnopharmacol. 2011;137(1):231–235.

[60] Ziauddin M, Phansalkar N, Patki P, et al. Studies on the immunomodulatory effects of Ashwagandha. J Ethnopharmacol. 1996;50(2):69–76.

[61] Jain J, Narayanan V, Chaturvedi S, et al. In vivo evaluation of Withania somnifera-based indian traditional formulation (Amukkara Choornam), against chikungunya virus-induced morbidity and arthralgia. J Evid Based Integr Med. 2018;23: 2156587218757661.

[62] Agbana YL, Ni Y, Zhou M, et al. Garlic-derived bioactive compound S-allylcysteine inhibits cancer progression through diverse molecular mechanisms. Nutr Res. 2020;73: 1–14.

[63] Goncagul G, Ayaz E. Antimicrobial effect of garlic (Allium sativum) and traditional medicine. J Anim Vet Adv. 2010; 9(1):1–4.

[64] Syu J-N, Yang M-D, Tsai S-Y, et al. S-allylcysteine improves blood flow recovery and prevents ischemic injury by augmenting neovasculogenesis. Cell Transplant. 2017;26(10): 1636–1647.

[65] Tauseef Sultan M, Sadiq Buttxs M, Nasir Qayyum MM, et al. Immunity: plants as effective mediators. Crit Rev Food Sci Nutr. 2014;54(10):1298–1308.